PROTEINS
STRUCTURE ■ FUNCTION ■ BIOINFORMATICS

Folding and dimerization of the ionic peptide EAK16-IV

Zhiqiang Yan, Jun Wang, and Wei Wang*

National Laboratory of Solid State Microstructure and Department of Physics, Nanjing University, 210093, China

ABSTRACT

Folding and dimerization of an ionic polyalanine-based peptide chain (EAK16-IV) are simulated with nonspecific interactions. It is found that there is a competition between two kinds of structural motifs under different strengths of electrostatic interactions. The dominance of hairpin-like structures would be realized with a strong electrostatic interaction both thermodynamically and kinetically, showing the importance of the electrostatic interaction on the formation of hairpin-like structures. Simulations on the dimerization with strong electrostatic interaction are also carried out. It is found that the concentration contributes essentially to the shape of the dimers. These studies demonstrate that the strong interactions and kinetic factors might be important for the ordered amyloid aggregates.

Proteins 2008; 72:150–162.

Key words: discrete molecular dynamics; hydrogen bond; electrostatic interaction; protein folding; aggregation.

INTRODUCTION

Biological cells are composed of very high concentrations of macromolecules such as proteins and so on.[1] In such a crowded environment, some ordered aggregates in the shape of amyloid fibrils are widely observed in biological systems.[1–4] It is suggested that such a kind of aggregation is a common feature of peptides and proteins.[5–7] Other abnormal aggregations are discovered to be a characteristic of many neurodegenerative-disorder-related diseases, such as Alzheimer's disease (AD), Parkinson's disease, Creutzfeldt-Jakob disease, and so on.[5–9] The exploration of the methods for the therapy of those diseases demands an extensive comprehension on the mechanism of the formation and propagation of amyloid fibril aggregates in such a complex cellular environment. Presently, the studies on the amyloid aggregation have become one of the most active areas in the researches on proteins.[10–12]

What is the main driving force of the irreversible aggregation? How do the ordered aggregates form through a self-organizing process? These questions are hotly discussed in research community, but the answers are still not totally clear.[10,13] The diverse spatio-temporal scales and the complex interactions in the amyloid aggregation make the understanding the molecular details of such a kind of processes difficult both in experiments and in simulations. As a rational approach, a series of model systems with the ability to form fibril aggregates are derived from real prion proteins or are constructed artificially.[14–21] These systems are generally composed of short peptides with specific compositions and simple interactions, and they maintain the fundamental features of the amyloid-related aggregation and largely ease the difficulties in the controlling and the analyzing of such complex processes. These model systems have become the regular objects in the studies of the amyloid aggregation. Besides, as a kind of self-assembling process, the formation of the ordered structures with these model peptides also attracts many attentions from other disciplines, such as physics and material science, on the underlying mechanisms and some possible applications of these nanoscale structures.[22]

The EAK-series peptides are a typical class of model systems in studying the formation of amyloid fibrils.[16–20] The reduced compositions, the ordered sequences of amino acids, and the simple interactions of the ionic EAK-series peptides make this kind of systems an appropriate and simple model in the studies on the aggregations processes and selfassembling of peptides, as well as the basic objects of our simulation approaches. These peptides are composed of three kinds of amino acids, the glutamic acid (E) carrying negative charge, the neutral alanine (A), and the lysine (K) carrying positive charge. These amino acids are often arranged with a certain order along the sequence. The residues E and K are aligned periodically. Based on the patterns of the

Grant sponsor: Foundation of NNSF; Grant numbers: 90403120, 10704033, 10774069, 10474041; Grant sponsor: National Basic Research Program of China; Grant number: 2006CB910302, 2007CB814806; Grant sponsors: FANEDD, NCET-05-0439.
*Correspondence to: Prof. Wei Wang, Physics Department, Nanjing University, Nanjing 210093.
E-mail: wei@nju.edu.cn
Received 6 May 2007; Revised 12 October 2007; Accepted 18 October 2007
Published online 23 January 2008 in Wiley InterScience (www.interscience.wiley.com). DOI: 10.1002/prot.21903

residues E and K, the regularly used EAK-series peptides include EAK16-I (with the sequence AEAKAEAKAEAKAEAK), EAK16-II (as AEAEAKAKAEAEAKAK), and EAK16-IV (as AEAEAEAEAKAKAKAK), respectively. The residues A are correspondingly used as the separators between the residues E and K to control the orientations of the side chains of the charged amino acids E and K. Because of the possible complementarity of the electrostatic interactions between these oligopeptides, these peptides could form fibril-like structures with rich ingredients of β-sheet-like structures at some proper conditions. It is worth pointing out that the EAK-series peptides maintains some common factors in the natural amyloid aggregates, such as the cooperation of different kinds of interactions as well as the competitions between monomeric stability and the multimeric tendency, though the compositions of EAK-series peptides are greatly simplified.

The EAK16-IV peptide is a typical example bearing all the characteristics of these model systems. Different from other EAK-series peptides, EAK16-IV could form a stable monomeric structure at proper conditions, which is valuable to help us understand the competition between monomeric and multimeric structures in the realistic self-assembling aggregations. More interestingly, EAK16-IV peptides could form different kinds of aggregate structures at various concentrations of peptides.[20] At the low concentration, the globular aggregates are formed, whereas only fibril aggregates appear at high concentrations. These features suggest that the EAK16-IV peptide is more informative in the family of EAK-series peptides. Our simulations would concentrate in such a peptide in this work.

There are many experiments on the aggregations of EAK16-IV peptides.[16–18,20] However, there are lacks in molecular descriptions for such processes. What kinds of interactions contribute most importantly for the aggregation? How does the fibril structure win during competition with various factors? To answer these questions, the simulations may provide more microscopic information. Presently, there are few simulation studies on the EAK16-IV peptide system, except that a worm-like chain model which emphasizes the competition between the electrostatics and the elasticity of the peptides is proposed to model the EAK16-IV peptides.[20] The atom-level architecture and the importance of the microscopic interactions (such as the hydrogen bonds) are not clearly considered. Besides, the effect of concentration on the formation of different structures was not considered explicitly in previous model. To consider the structural and environmental factors would give out a better understanding on the physics of the structural formations of this peptide system.

In this work, we model the EAK16-IV peptide with an intermediate-resolution model including the peptide planes and model side chains. The simulations both for the monomers and for the dimers of the peptide EAK16-IV are carried out with discrete molecular dynamics. It is found that the competition between the hydrogen interactions and the electrostatic interactions contributes importantly to the structural features of the monomer peptides. Different kinds of secondary structures would appear, depending on the pH condition of the solution which affects the electrostatic interactions. Following the decrease of the pH value, an helix-to-hairpin structural conversion is illustrated based on both the thermodynamic and kinetic information in our simulations, which is consistent with experimental observations.[23] During the dimerization of the EAK16-IV peptides, the concentration of the peptides greatly affect the population of the dimeric structures. The sheet-like dimers would have large probability to occur under the conditions with high peptide concentrations, while the systems with low protein concentrations would like to produce the dimers composed of the hairpin-like structures. This result demonstrates the kinetic selectivity for the dimeric structures by the concentrations of peptides. This may be helpful for understanding the diverse aggregate forms of the peptides EAK16-IV under different concentrations of peptides. These results demonstrate that both the interaction and the dynamic features are important for the formation of the aggregates of the EAK16-IV peptides, which might be a clue for understanding the formation of amyloid fibrils.

MODELS AND METHODS

Model for the EAK16-IV peptide

In EAK16-IV peptide systems with a large content of charged residues, both the hydrogen bonds and electrostatic interactions widely exist and contribute importantly to the stability and dynamics. These interactions are more important than the hydrophobic interactions for the monomeric and dimeric structures of this peptide, since there are no large hydrophobic amino acids in their compositions. To describe these interactions explicitly, a proper model with atomic information would be necessary.

In our simulations, a five-bead model for residues is used, in which the beads represent the α-Carbon (C_α), the carbonyl carbon (C) and oxygen (O), the amide nitrogen (N), and the first atom of side chain (C_β). In this model, all the heavy (nonhydrogen atoms) are explicitly represented except that the side chain of each residue is described by a single bead for simplicity. Different from the regular off-lattice models, the explicit inclusion of side chains may introduce proper chirality for amino acids as well as a more precise center for side-chain-related interactions.[24–26] It is worth pointing out that the polar hydrogen connected to nitrogen (N) can be calculated uniquely based on the rigid geometry of peptide plane. Therefore, this kind of model empowers an explicit representation for hydrogen bonds with the

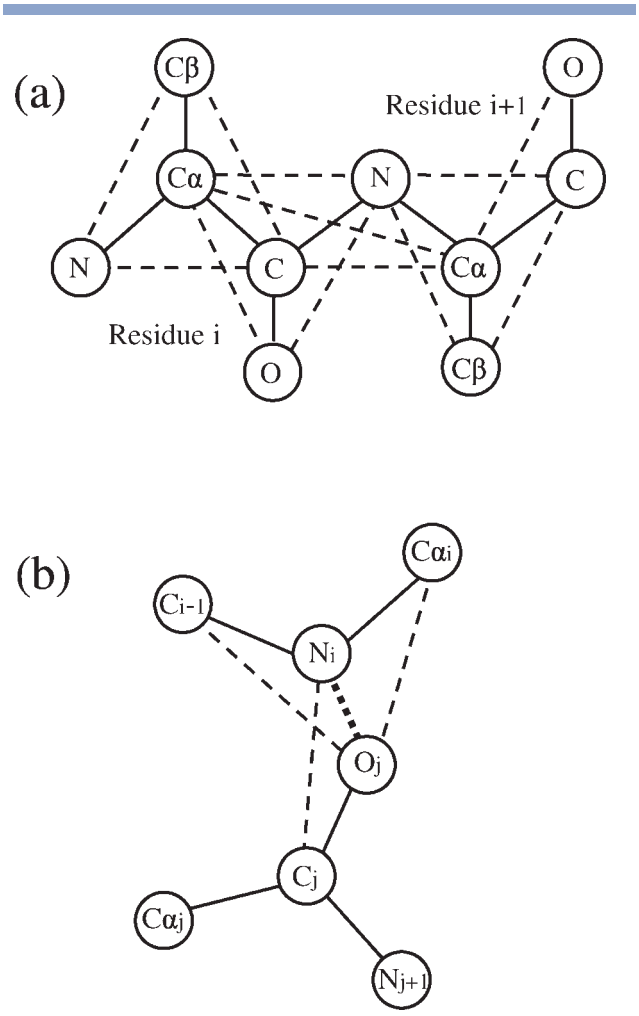

Figure 1

*(**a**) Schematic diagram of the five-bead model. The solid lines represent the covalent and the peptide bonds. The dashed lines represent the pseudo-bonds which are used to maintain backbone bond angles, consecutive C_α distances, and residue L-isomerization. (**b**) Schematic diagram of the hydrogen bond among backbone. The thick dashed line is the hydrogen bond, The thin dashed lines are the pseudo-contacts which are introduced to mimic the collinear structure of group CO and NH in real proteins.*

atoms C, N, and O in the peptide-bond plane. For simplicity, the masses of various beads are assumed to be the same m_0, which is the unit of mass.

Based on the five-bead representation of residues, the hamiltonian for the peptide systems has four parts of contributions, including the covalent binding between atoms H_{covalent}, the hydrogen bonds $H_{\text{H-bond}}$, the electrostatic interactions H_{elec}, and the hard-core repulsion of atoms H_{core}, that is,

$$H = H_{\text{covalent}} + H_{\text{H-bond}} + H_{\text{elec}} + H_{\text{core}} . \qquad (1)$$

The hydrophobic effect is not considered in present model as suggested above. The covalent interactions between atoms include the chemical bonds and the angular dependence of covalent binding, which are modeled with bond and pseudo-bond constraints, respectively.[26] In detail, there are five bonds and eight pseudo-bonds for a residue on average, which are shown in Figure 1(a) as solid and dashed lines, respectively. It is worth noting that the pseudo-bond $C_\alpha^i - C_\alpha^{i+1}$ is introduced to restrict the dihedral between the atoms C_α^i, C^i, N^{i+1}, and C_α^{i+1} and thus to ensure the planarity of peptide bonds. Here, i is an index for residues. Both the bond and pseudo-bond interactions are realized with infinitely high potential wells:

$$H_{\text{covalent}}(r_{\mu\nu}) = \begin{cases} 0, & 1-\delta < \dfrac{r_{\mu\nu}}{d_{s_\mu s_\nu}} \le 1+\delta, \\ \infty, & \text{otherwise}, \end{cases} \qquad (2)$$

where s_μ represents the type of the bead μ, $r_{\mu\nu}$ is the distance between beads μ and ν, d_{pq} is the bond length between the beads of types p and q, and δ is the tolerance of bond/pseudo-bond length which is regularly set as 0.02. The parameters $\{d_{pq}\}$ are chosen based on the data from crystal structures, which are listed in Table I. Similar parameters have been used in literature.[26]

Different from the bond or pseudo-bond interactions, the hydrogen bond behaves more complexly. The concerned atoms C, O, N and the related polar hydrogen prefer to have a collinear configuration due to the nature of the hydrogen bond. Here, we adopt a realization same as that in Ref. 27. The interaction of hydrogen bonds is modeled as a many-body interaction concerning the atoms N_i, C^{i-1}, C^i_α, C^j, and O^j [as shown in Fig. 1(b)], where i and j are indices of the donor and acceptor residues. In detail, we define four pseudo-contacts $N^i - O^j$, $N^i - C^j$, $C^{i-1} - O^j$, and $C^i_\alpha - O^j$. A pseudo-contact T is established when the distance D_T of two concerned atoms is within the corresponding range $[D_T^{\min}, D_T^{\max}]$, which takes the form

$$E_T = \begin{cases} 0 & D_T > D_T^{\max} \\ -1 & D_T^{\min} \le D_T \le D_T^{\max} \\ \infty & D_T < D_T^{\min} \end{cases} . \qquad (3)$$

With these pseudo-contacts, the hydrogen bond would come into being only when all the four pseudo-contacts are formed, that is

Table I

Parameters of Bond/Pseudobond Lengths in our Model

Bond (A)		Pseudo-bond (A)	
		$C^i - C^i_\beta$	2.494
$C^i_\alpha - C^i_\beta$	1.533	$N^i - C^i_\beta$	2.442
$C^i_\alpha - C^i$	1.510	$C^i - N^i$	2.444
$C^i_\alpha - N^i$	1.455	$C^i_\alpha - O^i$	2.394
$C^i - O^i$	1.222	$N^{i+1} - O^i$	2.248
$C^i - N^{i+1}$	1.325	$C^i_\alpha - N^{i+1}$	2.406
		$C^i - C^{i+1}_\alpha$	2.432
		$C^i_\alpha - C^{i+1}_\alpha$	3.784

Table II
Parameters of the Pseudo-Contacts Range for Hydrogen Bond

Pseudo-contact	$N^i - O^j$	$N^i - C^i$	$C^{i-1} - O^j$	$C^i_\alpha - O^j$
D^{min} (A)	2.80	3.80	3.60	3.60
D^{max} (A)	3.12	4.23	4.00	4.04

$$H_{\mathrm{H-bond}} = -\varepsilon_{\mathrm{HB}} \left| \prod_T E_T \right|, \qquad (4)$$

in which T runs over four pseudo-contacts mentioned above, and $\varepsilon_{\mathrm{HB}}$ is the strength of hydrogen bonds, which is taken as the energetic unit in our work. The detailed parameters for the pseudo-contacts are listed in Table II, same as those used in Ref. 27. Considering the complementary feature between the donor and the acceptor of the hydrogen bonds, at most one hydrogen bond is permitted for one carbonyl oxygen or one amide nitrogen in determining the hydrogen bonds. Besides, a minimal sequential distance (here 3) is required between hydrogen-bonded residues to mimic the local geometry of peptide chains.

Electrostatic interaction is another important non-bonded interaction in this system. In our model, the charge is placed at the center of the bead which mimics the side chain. Only the charge of glutamic acids and lysines are considered in our model. Considering the screening effect of solvent waters, a distance-dependent dielectric constant is employed as $\varepsilon_{\mathrm{dielec}} = 1/r$ where r is the distance between the concerned charges. Therefore, the electrostatic interaction would have the form of r^{-2}.[28] Since this kind of interactions decay rather slow, a multiple-step function is used,

$$H_{\mathrm{elec}}(r) = \begin{cases} 0 & r > d_M \\ u_k \varepsilon_{\mathrm{elec}} & d_k \le r \le d_{k+1}\ (k = 1, \ldots, M-1) \\ \infty & r < d_1 \end{cases}, \qquad (5)$$

in which $\varepsilon_{\mathrm{elec}}$ is the strength of electrostatic interaction, the distance set $\{d_k\colon k = 1,\ldots,M\}$ describes the location of steps, and u_k $(k = 1,\ldots,M-1)$ is the corresponding energetic parameter. In our model, $M = 6$ steps are chosen, and the corresponding parameters $\{d_k\}$ and $\{u_k\}$ are given in Table III, which are determined by fitting the function r^{-2}. The strength $\varepsilon_{\mathrm{elec}}$ depends on the charges of the concerned residues. Thus, the strengths between residues E and K would be negative, and those between residues of same type would take positive values. For simplicity, we think that the attractions and the repulsions have a same magnitude of strength $|\varepsilon_{\mathrm{elec}}| = \chi$. It is worth noting that the strength of electrostatic interaction depends on the environment conditions, such as pH values of the solution, since the charges of amino acids and the related interactions may be affected by the solutions. For example, in the acidic solutions, the increase of ion concentration would enhance the screening effect which would decrease the attraction or repulsion between charges. More complexly, some residues may change their protonization state which changes the partial charges of the residues. In consequence, the strength $\varepsilon_{\mathrm{elec}}$ would decrease comparing with that in the neutral condition. In our work, we phenomenologically simulate various pH conditions by controlling $\varepsilon_{\mathrm{elec}}$. A large strength corresponds to the case near the neutral condition, and the small strengths are used to mimic the acidic or basic condition. The similar considerations have applied in some modeling for the effect of denaturants.[29]

Besides the above interactions which concern some specific atoms, the hard-core interaction is unique for every pair of atoms to realize the exclusive-volume effect. The hard-core interaction between the atoms μ and ν generally has the form

$$H_{\mathrm{core}}(r_{\mu\nu}) = \begin{cases} 0 & r_{\mu\nu} > R_{\mathrm{core}} \\ \infty & \text{otherwise} \end{cases}, \qquad (6)$$

where R_{core} shows the size of repulsive core, and is regularly determined as the summation of the radii of the concerned atoms, $R_{\mathrm{core}} = R_\mu + R_\nu$. The radii of various atoms are presented in Table IV.

Different from the model used in the reference,[20] the coarse-grained bending term is not included explicitly in our model. Instead, a series of atom-level interactions are employed in our hamiltonian, Eq.(1). This kind of consideration not only successfully reproduces the local geometry and elasticity focused by the bending term in the worm-like chain model, but also bring us a better way to describe the structural details and competitive interactions of the peptide system, such as the turn structure of the hairpin-like monomers, the planar organization in the dimeric structures due to the directional hydrogen bonds and so on, which cannot be clearly outlined based on the coarse-grained worm-like chain models.

Table III
Parameters of Steps Location and Corresponding Energy for Electrostatic Interaction

k	1	2	3	4	5	6
d_k (A)	4.4	4.8	5.7	6.8	9.2	15.0
u_k (ε_{HB})	1.00	0.77	0.54	0.33	0.14	

Table IV
Parameters of Hard-Core Radii for Various Atoms

Atom	C_α	C	N	O	C_β
Radius (A)	1.85	1.60	1.55	1.00	2.20

Discrete Molecular Dynamics

Compatible with our discontinuous potentials, the event-driven discrete molecular dynamics (DMD)[30–33] are used in our simulations. The collisions and propagations of the beads are processed sequentially, and all these events build up the dynamics of systems. The discontinuous feature of potentials makes the propagation be the motion with constant speed, and thus, the processing of the events all are algebra calculations rather than the integration of dynamic equations, which greatly reduces the computational demands. It is worth noting that the event-driving feature makes the time of evolution is not a counting of the number of the collisions, but a summation of times of all propagations. The time unit is defined as $\tau_0 = \sigma_0\sqrt{m_0/\varepsilon_{HB}}$, where σ_0 is the unit length (= 1Å). In our DMD simulations, constant-temperature ensemble is realized with the Andersen's method.[25,34,35] The number of the collisions with ghost particles is controlled as about 1% of all collisions, which ensures the thermodynamic equilibrium.

Weighted Histogram Method

Weighted histogram method is employed to calculate the thermodynamic properties.[35,36] In this method, a series of histograms obtained from thermodynamic sampling could be utilized together to find out the density of states and partition functions based on a self-consistent method. With this kind of method, the statistical errors could be minimized, which greatly extends the validity of results for a large range of temperatures. For our discontinuous potential, we generally take the minimal interval (often 0.1) of energy spectrum as the bin size of the histograms.

RESULTS AND DISCUSSIONS

Folding of EAK16-IV peptide monomers

As suggested by some previous works on dimerization and aggregation of proteins,[37,38] the folding feature of the corresponding monomers is important for understanding the further complex organizations. In our work, the thermodynamics and kinetics of a single chain of EAK16-IV peptide at various temperatures and with different electrostatic strengths are obtained through a series of DMD simulations. The preferences to some certain secondary structures on various conditions are illustrated, which shows the complex competition of interactions in this model system.

In our work, a series of DMD simulations of the model peptide are performed at various temperatures (ranging from T = 0.06 to 0.20) and electrostatic strengths (from χ = 0.0 to 0.5). Some typical trajectories are shown in Figure 2. It is observed that there are three categories of microscopic states along the trajectories. These categories have apparent difference in the arrangement of their hydrogen bonds. Based on the pattern of hydrogen bonds, these structures are named as $\mathcal{H}$-type (with rich α-helix content, namely with a lot of hydrogen bonds between ith and i + 4th residues), $\mathcal{P}$-type (with plenty of β-hairpin-like structures, namely with the ladder-like pattern of hydrogen bonds) and $\mathcal{C}$-type (extended or with some random hydrogen bonds). The structure with the minimal energy in the $\mathcal{H}$-type category or in the $\mathcal{P}$-type category is picked out as the representative structure of the corresponding category. These representative structures are shown in Figure 3. The representative structure for $\mathcal{H}$-type category is a α-helix with totally 12 hydrogen bonds [as Fig. 3(a)]. Meanwhile, the representation structure for $\mathcal{P}$-type category is a hairpin-like structure containing 6 hydrogen bonds [as shown in Fig. 3(b,c)]. It is worth noting that this hairpin-like structure has an unusual five-residue turn which makes the side chains of residues E and K point to the same side of the hairpin, which has been observed in FTIR spectrum.[20] With these representative structures, the corresponding categories are defined more specifically as the set of the structures with at least 2/3 of total hydrogen bonds of the representative structures.

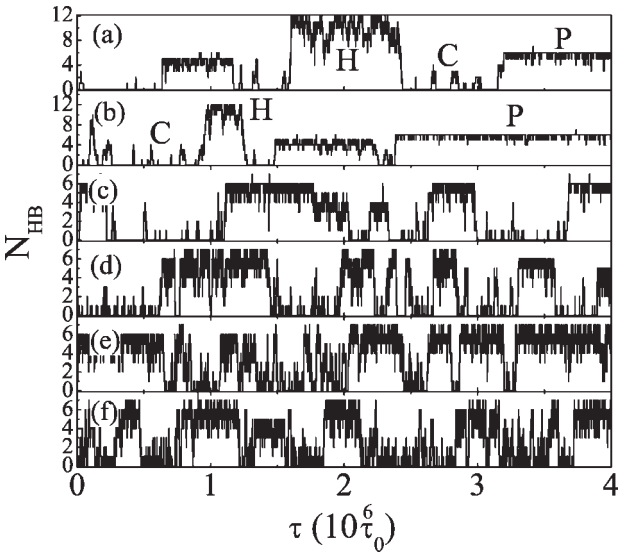

Figure 2

*Trajectories with the occurrence probability of C states as around 0.5. (**a**) χ = 0.00, (**b**) χ = 0.10, (**c**) χ = 0.20, (**d**) χ = 0.30, (**e**) χ = 0.40, (**f**) χ = 0.50.*

When the electrostatic strength χ is not larger than 0.2, both the $\mathcal{H}$-type and the $\mathcal{P}$-type structures could be observed at some proper temperatures [as shown in Fig. 2(a,b)]. It is interesting to find out that there are no direct transitions between $\mathcal{H}$-type states and $\mathcal{P}$-type states. The model peptide has to pass the extended $\mathcal{C}$-type states to switch between $\mathcal{H}$- and $\mathcal{P}$-type states. This could be attributed to the large distinction between the

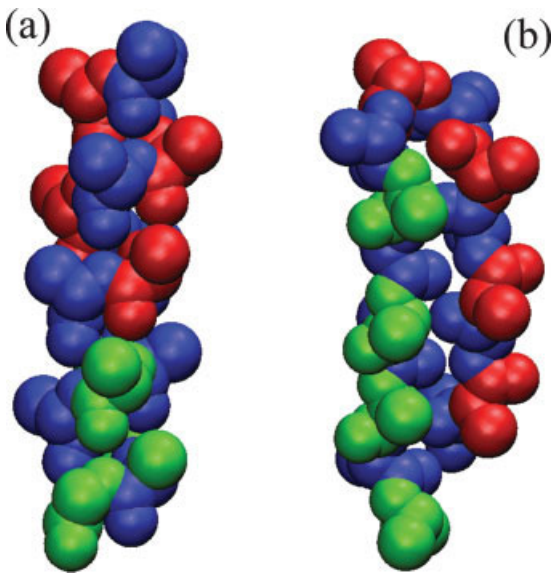

Figure 3

*Snapshots of a full α-helix conformation (**a**) which has 12 α-helical hydrogen bonds with four α-helical turns, and a hairpin-like conformation with a five-residue turn located at the center (**b**). These conformations are colored based on the residue types, red for E, blue for A, and green for K. The structures are shown with five-bead model plotted by VMD software package.*

patterns of hydrogen bonds for these two kinds of states. The large differences on their geometrical shapes also prevent the existence of the intermediates sharing by both characteristics of $\mathcal{H}$-and of $\mathcal{P}$-type states. It seems that the helical structures and hairpin structures constitute two separated funnels on the energy landscapes. This large separation between these two kinds of structures suggests that a high temperature and a sufficient incubation time are necessary for the β-to-α conversion, which has been observed in experiments.[16]

For larger χ than 0.1, no $\mathcal{H}$-type conformations are obtained during our simulations. Here, to validate the comparison, all the trajectories have the occurrence probability of $\mathcal{C}$-type states as ≈0.5. This kind of selections for the structural motifs originates from the different compatibility of the electrostatic interactions with $\mathcal{H}$ and $\mathcal{P}$ states. The positive and negative charges distribute separately on two half of the peptide chain. The attraction between different types of charges would only be helpful for the hydrogen bonds in the middle of the helix. The repulsion between the same type of charges would make the hydrogen bonds at both *N* and *C* termini unstable. Differently, the charges on the two arms of hairpin are complementary, and, thus, the energy of H_{elec} is greatly minimized, so that the hairpin structure is further stabilized by electrostatic energy. As a result, the introduction of the electrostatic interaction would pave the funnel related to $\mathcal{H}$-type structure, deepen the well related to $\mathcal{P}$-type structures, and produce the observed bias in conformational space.

This kind of preference has been observed in experiments.[16–18] There are strong β-sheet circular dichroism (CD) signal at the neutral environment for the EAK16-IV peptides in very dilute solutions which favors the monomeric structures. There are not CD signal for helix on this condition. Besides, the helical structures obtained by heating could return to β-type structure after sufficient long time, which implies that the β-type structure is more stable on regular conditions. This kind of preference is also widely observed for other peptides with the same charge distributions.[17] Surely, the preference for this kind of peptides may be affected by the pH value of the peptide solution.[17] Apparent CD signal for helix may be observed in the peptide solutions with a small pH value. This regularly happens for rather low pH values, namely with rather small strength of electrostatic interaction. This is consistent with the case with small electrostatic strength χ, and further supports the observations from simulations that a small extent of electrostatic interaction could greatly suppress the helical structures ($\chi \leq 0.2$). Both the simulations and experiments suggest that the electrostatic interaction is the main factor to affect the monomeric structural features.

Based on the observation on dynamic processes, the peptide system behaves rather more complex than the regular proteins with unique native structures. To have a more systematic picture for such a system, the thermodynamic features are evaluated with the weighted histogram method based on the simulations at various temperatures. The temperature dependence of heat capacities for various electrostatic strengths χs are shown in Figure 4(a). Same as their dynamics, the heat capacity also behaves not trivially. For the case of $\chi = 0$, there is one high peak for the heat capacity. When slightly increasing the strength of electrostatic interaction to $\chi = 0.1$, two peaks appear in consequence. Further increasing of the strength χ, the heat capacity would recover the single-peaked form. Investigating the sampled structures more detailedly, it is found out that these transitions are not all the same. The transition at $\chi = 0$ corresponds to a large energy jump between $\mathcal{C}$-type states and $\mathcal{H}$-type states, while the single peaks at large χ act as the separator between coil-rich $\mathcal{C}$-type states and the hairpin-dominated $\mathcal{P}$-type states. More interestingly, the twin peaks for small χ are not the combination of the above two cases, and correspond to the $\mathcal{C}/\mathcal{P}$ (at the high temperature) and $\mathcal{P}/\mathcal{H}$ (at the low temperature) transitions, respectively. These behaviors shows up the complexity in the ionic peptide systems.

Considering the features of the backbone entropy of the helix and of the hairpin,[26] the free energies of the $\mathcal{H}$-type, of $\mathcal{P}$-type and of $\mathcal{C}$-type states are given out to explain the variations of the heat capacities [as shown in Fig. 4(b-d)]. When $\chi = 0$, the free energies of the three

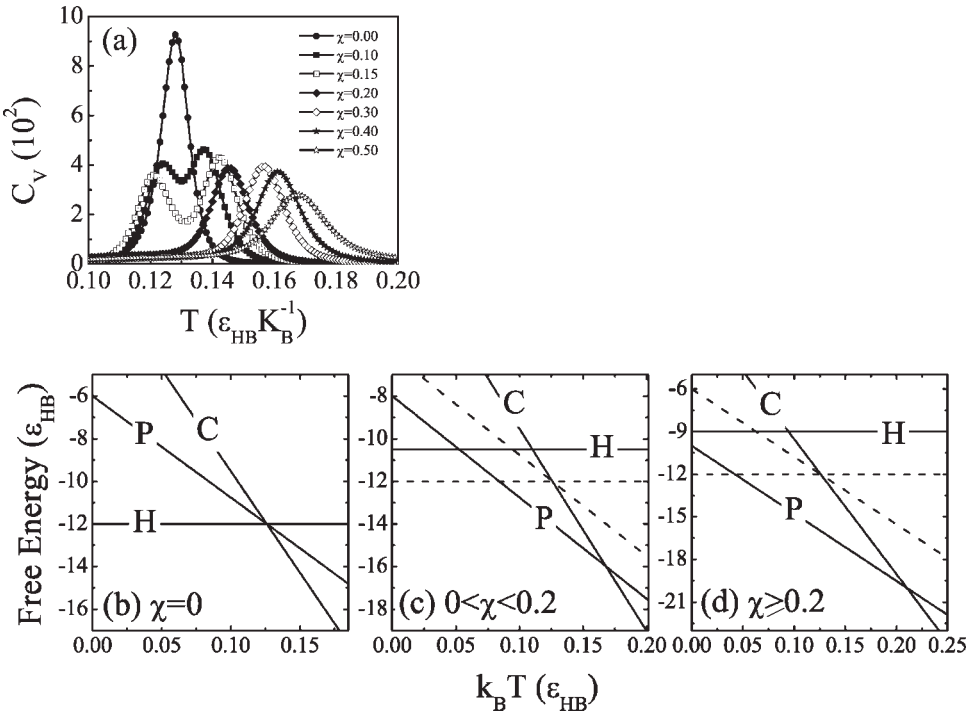

Figure 4

*(**a**) gives out the heat capacity C_v as a function of reduced temperature for different χ values (0, 0.1, 0.15, 0.2, 0.3, 0.4, and 0.5) with a weighted histogram method. The free energies of $\mathcal{H}$-, $\mathcal{P}$-, and $\mathcal{C}$-type state at (**b**) $\chi = 0$ (**c**) $0 < \chi < 0.2$ (**d**) $\chi \geq 0.2$ are given. The dashed lines in (c) and (d) is used as a reference, which correspond to the case $\chi = 0$.*

states would almost intersect at a same point [as shown in Fig. 4(b)], which produces a single observable transition. Comparing the sizes of their free energies, this transition could be regarded as the one between the $\mathcal{C}$-type states and $\mathcal{H}$-type states. In fact, at the transition temperature, both the $\mathcal{C}/\mathcal{H}$ transition and the $\mathcal{C}/\mathcal{P}$ transition happen concurrently, but the $\mathcal{P}$-type state is generally the meta-stable state in both phase. In the literature,[26] Ding and his colleagues also discovered the approximate equality between the temperature of the $\mathcal{C}/\mathcal{P}$ and that of $\mathcal{C}/\mathcal{H}$ transitions for the poly-alanine system. Our results for the case $\chi = 0$ approve this conclusion. When $0 < \chi \leq 0.2$, the hairpin-like structures become more stable and the helix structures are destabilized following the increase of χ. Correspondingly, the free energy for the $\mathcal{P}$-type states would move downward and that of the $\mathcal{H}$-type states would move inversely. In this stage, there are two intersection points between these three lines, which corresponds to two peaks of the heat capacities and suggests two structural transitions. The peak at the high temperature corresponds to the $\mathcal{C}/\mathcal{P}$ transition, and the one at the low temperature is related to $\mathcal{P}/\mathcal{H}$ transition. Below the temperature related to the $\mathcal{C}/\mathcal{H}$, the $\mathcal{H}$-type state becomes a meta-stable state more stable than random coil states, which could be observed in dynamic simulations. With larger χ ($\chi \geq 0.2$), the free energies of these three states would vary in a same manner. In this situation, the transition between $\mathcal{C}$-type states and the $\mathcal{P}$-type states would not change except that the transition temperature becomes larger following the increase of χ. The transition between $\mathcal{P}$-type states and $\mathcal{H}$-type states would disappear since the helix is less stable than the hairpin even at the temperature $T = 0$. The helix would always be a meta-stable state at low temperature (lower than the $\mathcal{C}/\mathcal{H}$ transition temperature). In consequence, the heat capacity would recover to be a unimodal one. This kind of non-monotonic behaviors demonstrate the competition of the helical and the hairpin structures controlled by the strength of the electrostatic interaction.

As expected, the critical temperatures for the $\mathcal{C}/\mathcal{P}$ transition and for $\mathcal{P}/\mathcal{H}$ transition, which are determined from the peaks of the heat capacities, vary almost linear with the strength χ (as shown in Fig. 5), which clearly illustrates the dominant effect of the electrostatic interaction for the variation of the transitions. More interestingly, the destabilization of the $\mathcal{H}$-type category at large χ would move some microscopic states into the $\mathcal{C}$-type category. The enlargement of the ensemble of the $\mathcal{C}$-type structures would affect the balance between the $\mathcal{C}$- and $\mathcal{P}$-type states. The variation of the related transition tem-

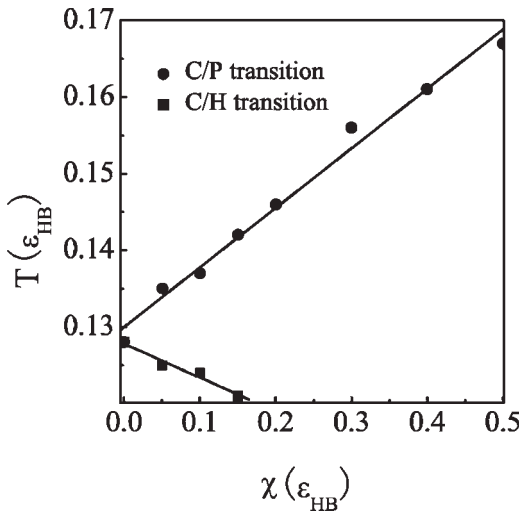

Figure 5

The transition temperatures T_T for different χ values. The lines are guide for eyes.

peratures at large χ would slightly bend down due to the entropic increase of the $\mathcal{C}$-type states (as shown in Fig. 5). The cooperativity of the $\mathcal{C}/\mathcal{P}$ transition is also slightly deteriorated due to the broadening of the denatured states($\mathcal{C}$-type states)[39] as suggested from the broadening and shortening of the peak of heat capacity.

Clearly, the variation of the energy landscape of such a peptide with a nonspecific interaction is more complex than the regular proteins modeled by Gō-like interactions. The present thermodynamic analysis brings us a better picture for the variation of the landscapes related to the change of electrostatic interaction.

Besides the thermodynamic competitions between various structural motifs, another interesting issue for model peptide system is the dynamic behavior under a quenching condition which is often realized in experiments for aggregation or structural formation. This kind of processes is often related to kinetic partition rather than the thermodynamic competitions. It is another interesting aspect which might be important to understand the nonequilibrium dynamics of this kind of systems. Here, we would concentrate into the quenching processes at low temperatures. Based on our above thermodynamic simulations, the $\mathcal{P}/\mathcal{H}$ transition and the $\mathcal{C}/\mathcal{P}$ transition often happen at the temperatures higher than $T_T = 0.12$. Therefore, we carry out our simulations for the quenching processes from 0.06 to 0.1 which are apparently lower than T_T. In these quenching processes, the peptide would not always fold to their ground state due to the ruggedness of the landscape, and may be frozen in the $\mathcal{H}$-type or $\mathcal{P}$-type category. In our simulations, the freezing behaviors are identified when the system resides on a certain state for a rather long time (practically 10^6 τ_0). This period is rather longer than the mean first arrival times (MFAT) at low temperatures to the $\mathcal{H}$-type states (typically $0.7 \times 10^5\tau_0$ at $T = 0.9$) and $\mathcal{P}$-type states (typically $0.4 \times 10^5\tau_0$ at T 0.9). The MFAT for different low temperatures vary slightly for this short peptide. The frozen conformations could be classified into $\mathcal{H}$-type and $\mathcal{P}$-type based on their categories. With about 200 trajectories starting from random extended coils for each temperature, a series of frozen conformations are collected, and the probabilities of the $\mathcal{H}$-type and $\mathcal{P}$-type frozen conformations are calculated. The results demonstrate the kinetic preference toward some certain structural motifs (as shown in Fig. 6). It is found that the probability $Q^{\mathcal{H}}$ (or $Q^{\mathcal{P}}$) is approximately independent of the temperature. For a certain electrostatic strength, the probability is almost invariant for different temperatures. This suggests that the kinetic partition depends weakly on the temperature. On the other hand, following the increase of electrostatic strength, both probabilities $Q^{\mathcal{H}}$ and $Q^{\mathcal{P}}$ vary monotonically. $Q^{\mathcal{H}}$ goes down from about 0.7 to 0.0, while $Q^{\mathcal{P}}$ increase from 0.15 to about 0.9. For small strength χ, the probability to have $\mathcal{H}$-type conformations is much larger than that for $\mathcal{P}$-type conformations, which suggests that there is a larger entry to form the helical structures than that to hairpin-type structures. This consists with the common idea that the helix could be initiated from many local hydrogen bonds while the formation of hairpin regularly concerns the stabilization of a specific turn structure. It is interesting to notice in

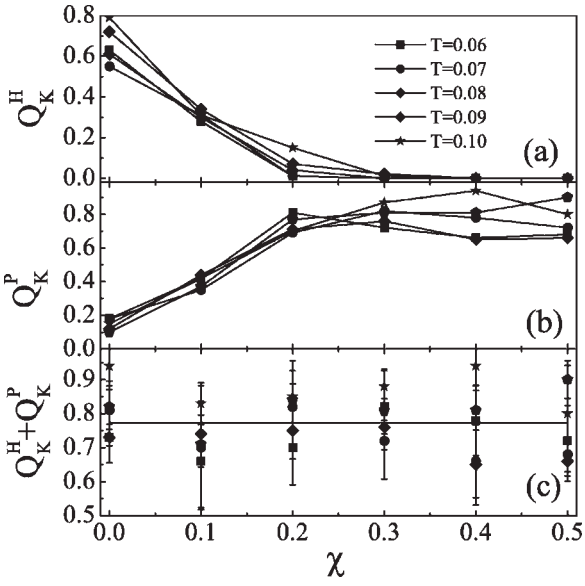

Figure 6

Probabilities to be trapped into a certain type of structure, $Q_k^{\mathcal{H}}$ (for $\mathcal{H}$-type structures) and $Q_k^{\mathcal{P}}$ (for $\mathcal{P}$-type structures) at the temperatures from $T = 0.06$ to 0.1.

both experimental and simulation studies[40–44] that the helical structures often form faster than beta structures. Sometimes, beta structures may have the intermediates with helical contents. These indicate that the helical structures are easier to form than beta-structures in kinetics. Consistently, in our simulations with $\chi = 0$, the helical structures have a much larger probability to occur than that of the beta structures at low temperatures. Our results demonstrate the kinetic preference to the helical structures For the large electrostatic interactions, the situation is different. When $\chi \geq 0.3$, the system prefers to form $\mathcal{P}$-type conformations, and the helical structures even disappear in our samples. This also demonstrates the bias of the electrostatic interaction toward the $\mathcal{P}$-type structures, consistent with the above thermodynamic analysis. It is worth noting that the summation $Q^{\mathcal{H}} + Q^{\mathcal{P}}$ is almost constant for various χs [as shown in Fig. 6(c)]. The variations of two probabilities are nearly synchronous. This kind of variation of the populations of different structural motifs demonstrates the competition between them and suggests the importance of the electrostatic interaction selection of conformations.

Formation of dimers of EAK16-IV peptides

With the nonspecific hydrogen bonds and electrostatic interactions, multiple EAK-peptide could form much more complicated structures. Dimeric organization of EAK16-IV peptides is one of complex structures with EAK16-IV peptides, which acts as the basic part of further architectures. It is also the simplest organization with multiple peptides, which shares some common features of complex structure formation. In this work, we carry out a simulation study on the dimerization of EAK16-IV peptides. The contribution of the concentration of peptides is described, and is used to explain some experimental observations[20] that the nanostructures formed by EAK16-IV change from globules to fibrils as the concentration increases.

Same as the system with a single peptide, both the hydrogen bonds and electrostatics are considered in nonbonded interaction of dimeric system. Referring to the experiment-interested conditions which favors the fibril formation, we fix the strength χ of electrostatic interaction at a large value 0.5. Under this situation, the hairpin structure is preferred both in thermodynamics and in dynamics. With these kinds of interactions, the simulations for the dimerization of two chains of EAK16-IV peptides are carried out in a cubic box of edge L with a periodic boundary. A proper concentration C of peptides is realized by controlling the edge size L, that is, $C = 2/N_A L^3$, where N_A is the Avogadro constant. In our work, we simulated a series of sizes of edge, as 40, 45, 50, 60, 70, 75, 80 Å, which correspond to the concentrations from 52 mM (corresponds to $L = 40$ Å) to 6.5 mM (corresponding to $L = 80$ Å). Because of the effect of large translational entropy as well as the rugged landscape, it is difficult to have a thorough thermodynamic analysis. Here, we concentrate in the dynamics of dimerization instead of the thermodynamics. In our simulations, we practically define a dimer when there are at least 4 interchains hydrogen bonds (a quarter of the maximal number of inter-chain hydrogen bonds) formed, which ensures the sufficient stability of the dimeric structures. The simulation temperature is taken as $T = 0.14$. At this temperature, the system could form stable dimers fast. For example, after a period of $4 \times 10^5 \tau_0$, about 95% trajectories could reach stable dimeric structures for a typical concentration ($L = 60$ Å). High temperatures may decrease the probability to form dimers, while low temperatures would weaken the mobility of the peptides and make the simulation be frustrated in the energetic traps. This consists with the temperature dependence of the monomeric structures since the same interactions are involved in both processes, and supports the observation that the temperature could sensitively control the shape and quality of fibril aggregations.[21]

Under these conditions, two EAK16-IV peptides are put into the box with random extended conformations, and the initial distance between their centers of mass is nearly half of edge size L which is the largest distance for such a box. Because of the large transitional entropy, not all runs can result in the dimeric conformations. The ratio P_D to have dimeric structures within the period $4 \times 10^5 \tau_0$ is clearly a concentration-dependent quantity (as shown in Fig. 7). High concentrations (namely small free space) would make the chains easy to meet each other and to have more chances to bind together. Quantitatively, the ratio saturates exponentially with the concentration. That is, the residual ratio P_{UD} with no dimeric structures formed decreases exponentially (as shown in the inset of Fig. 7). For a simple barrier-crossing process, the logarithm of the residual population is regularly proportional to the time of barrier-crossing dynamics. Therefore, we could speculate that the dimerization rate increases linearly with the concentration. It consists with the linear decrease of the free-energy barrier of binding which comes from the cease of the translational entropy.

Different from the regular folding, the dimers of the peptide system do not have a unique "native" structure with the largely nonspecific interactions. Considering the difference of the patterns of intra- and interpeptide hydrogen bonds, the dimeric structures could be classified into two types, sheet type (named as $\mathcal{S}$-type) and hairpin type (as $\mathcal{P}$-type). The main difference between these two types is that the $\mathcal{S}$-type dimers have no intrapeptide hydrogen bonds while the $\mathcal{P}$-type dimers are built from the hairpin structures (typical conformations as shown in Fig. 8). In fact, there are many kinds of arrangements for these two types of dimers since there are no chemical connectivity restricting their shapes. For example, both parallel and antiparallel sheets may appear

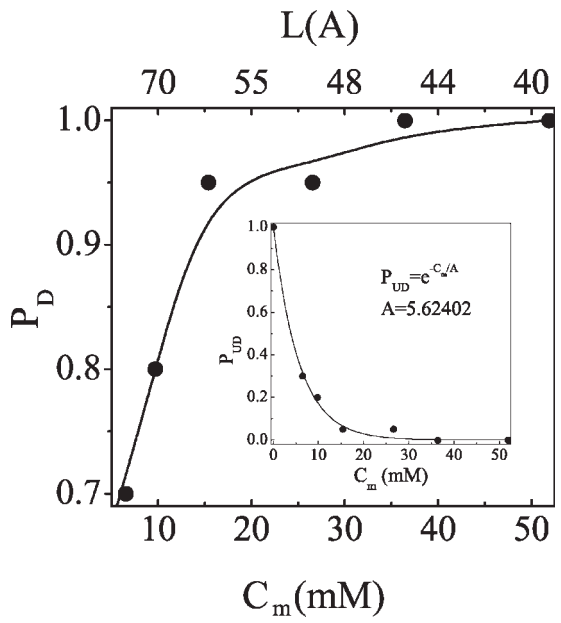

Figure 7

The probability P_D to form a dimeric structures in various concentration. The corresponding sizes of simulation boxes is shown as the top label. The line is used as a guide for eyes. The residual probability P_{UD} is shown in the inset and is fit with an exponential function with A = 5.62.

for $\mathcal{S}$-type dimers. For large concentrations, some peptides may have cross-links with the image peptide in the neighbor box, and form more complex sheet structures. Anyhow, these structures are all the stable local minima on the energy landscape though the $\mathcal{P}$-type dimeric structures are less stable with more structural fluctuations (data are not shown). The existence of a large number of stable conformations suggests that the landscape for the dimeric system is more rugged than that of monomeric peptide. It is interesting to notice that all the dimeric structures (both $\mathcal{S}$-type and $\mathcal{P}$-type) are planar. It is easy to speculate that the large-scale organization of the EAK16-IV peptide may also possess this kind of planar feature. This kind of guess has been verified by the AFM experiments.[18] The filament, the fibril, and the thinnest globule aggregates all have the same height which approximately equals to the thickness of the above planar structures. This kind of behavior is probably the contribution of the hydrogen bonds, since the electrostatic interactions are generally isotropic and have not preferential directions. This implies that the hydrogen bonds are not neglectable though the electrostatic interaction is essential in energetics for the peptide system. Indeed, the planar organization induced by hydrogen bonds may prevent random packing of monomers and provide some preferential growth direction, which would be a basic step for the fibril formation. This also demonstrates the possible importance of hydrogen bonds in fibril growth.

Another interesting issue is the different stability of two types of dimers. It is easy to find out that $\mathcal{P}$-type dimers have more pairs of electrostatic attractions and hydrogen bonds than the $\mathcal{S}$-type dimers. A plausible speculation would be that the $\mathcal{P}$-type dimers would be more stable than $\mathcal{S}$-type dimers. To check the stability of these two types of dimers, we carry out some computational folding and unfolding for the representatives of these two types of dimeric structures, antiparallel β-sheet [as shown in Fig. 8(a)] and antiparallel β-hairpin [as shown in Fig. 8(d)], which are the most stable ones of their own types. The average times τ_{uf} from the selected dimeric structures to the totally unfolded structures (namely with no hydrogen bonds) and the mean first arrival time τ_f from random structures to the corresponding type of dimers and are calculated (as shown in Fig. 9). The melting temperatures for the concerned dimers are determined as the ones satisfying $\tau_{uf} = \tau_f$. It is found out that the melting temperature for $\mathcal{S}$-type dimers is apparently larger than that for the $\mathcal{P}$-type dimers. That is, $\mathcal{S}$-type dimers are more stable than $\mathcal{P}$-type dimers, which contradicts with the above intuitive guess. At the temperature 0.170, we even observe a fast conversion from $\mathcal{P}$-type dimers to the $\mathcal{S}$-type dimers [as shown in Fig. 10(a)] with a cease of hydrogen bonds inside of chains and a corresponding increase of the hydrogen bonds between chains. it is worth noting that the folding times of dimers varies not sensitively on the type of dimers (as shown in Fig. 9), which consists with the above analysis on the binding rate. With this knowledge, it is also possible to judge the stability of dimers simply based on the size of unfolding times, which has been used in judgment of stability of amyloid-related peptide oligomers.[45]

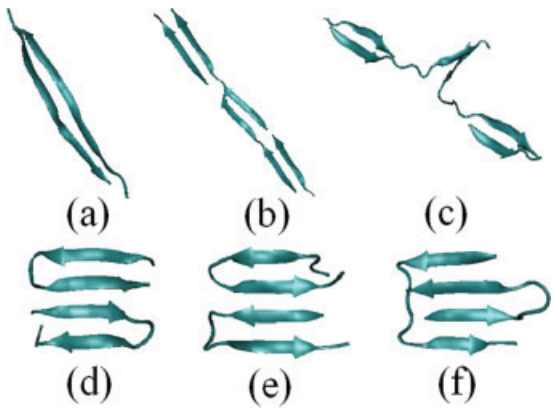

Figure 8

*Typical dimeric structures for EAK16-IV peptide, (**a**) antiparallel β-sheet dimer, (**b**) parallel β-sheet dimer, (**c**) mixed β-sheet dimer, (**d**) antiparallel β-hairpin dimer, (**e**) parallel β-hairpin dimer and (**f**) mixed β-hairpin dimer. a, b, c are classified into $\mathcal{S}$-type dimer, and d, e, f are $\mathcal{P}$-type dimer. [Color figure can be viewed in the online issue, which is available at www.interscience.wiley.com.]*

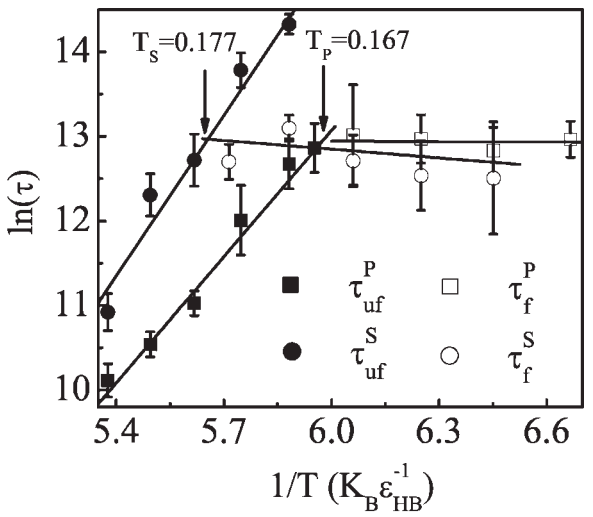

Figure 9

The unfolding time τ_{uf}^{X} of the X-type dimer and the MFAT τ_{f}^{X} from random monomers to X-type dimers are shown. Here, X means $\mathcal{S}$ or $\mathcal{P}$. The melting temperatures corresponding to the intersection of τ_{uf} and τ_f are also given out as 0.177 for $\mathcal{S}$-type dimers and 0.167 for $\mathcal{P}$-type dimers.

What is the reason to have this surprising result? Some detailed investigations on the unfolding trajectories provide us more information. For the $\mathcal{S}$-type dimers, the unfolding is cooperative with a sharp change of the number of hydrogen bonds [as shown in Fig. 10(c)], which shows a dynamics in a two-state manner. Differently, the $\mathcal{P}$-type dimers behave with multiple steps. The breakup of the inter- and intrachain hydrogen bonds are not synchronous [as shown in Fig. 10(b)], regularly first interchain part and then the intrachain part, though the destructure of each part is also cooperative. That is to say, the intra-peptide hydrogen bonds would not contribute to the stability of the dimers. Since the interaction between two monomers of the $\mathcal{P}$-type dimers is apparently weaker than that of the $\mathcal{S}$-type dimers, the $\mathcal{P}$-type dimers are not so stable as $\mathcal{S}$-type dimers in their dimeric form. As a result, the unfolding of $\mathcal{P}$-type dimers would have a large dissociation rate, and exhibit a weak stability. This kind of instability also explains the observable fluctuation of the $\mathcal{P}$-type dimeric structures. In this sense, the stability of the dimers seems to be more relevant to the interaction between two monomers, rather than the total energetics which include the contribution of the monomers. This is also true for the systems which could form fibrils.[5,7]

Besides the temperature, two types of dimers have different responses to the variation of concentration of peptides. The probability $P^{\mathcal{S}}$ or $P^{\mathcal{P}}$ to reach the $\mathcal{S}$-type or $\mathcal{P}$-type dimers is calculated for various concentrations. It is found that these probabilities are not constant for various concentrations of peptides (as shown in Fig. 11). The probability $P^{\mathcal{S}}$ increases almost linearly while the probability $P^{\mathcal{P}}$ decreases also almost linearly. Obviously,

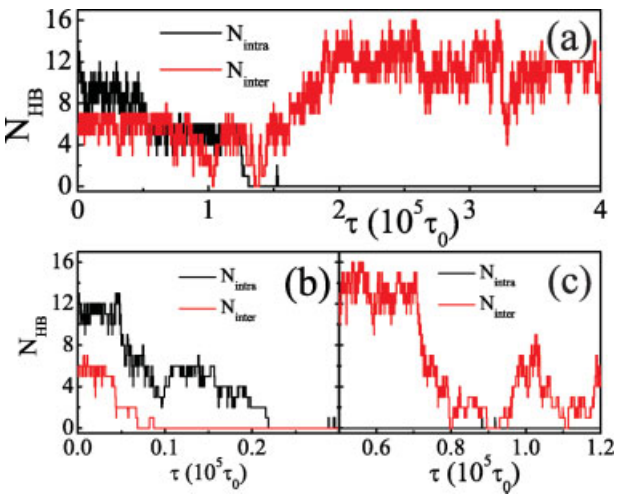

Figure 10

*Unfolding trajectories monitored by the numbers of hydrogen bonds, N_{intra} (inside the peptide chains) and N_{inter} (between peptides). Several typical conditions are given, (**a**) a conversion from a $\mathcal{P}$-type dimer to $\mathcal{S}$-type dimer at $T = 0.170$, (**b**) and (**c**) the unfolding of $\mathcal{P}$-type and $\mathcal{S}$-type dimers at $T = 0.180$. [Color figure can be viewed in the online issue, which is available at www.interscience.wiley.com.]*

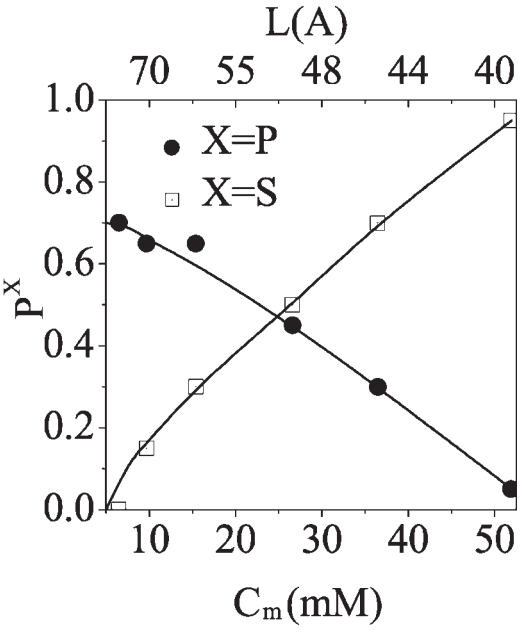

Figure 11

The probabilities $P^{\mathcal{S}}$ and $P^{\mathcal{P}}$ to have $\mathcal{S}$-type dimers and $\mathcal{P}$-type dimers at various peptide concentrations. The corresponding sizes of the simulation boxes are shown as the top label. The lines are the guides for the eyes.

at the small concentrations, $P^{\mathcal{P}}$ is always larger than $P^{\mathcal{S}}$. Differently, at the high concentrations, they would change their places with a large $P^{\mathcal{S}}$ and a small $P^{\mathcal{P}}$. The dilute solutions prefer to the $\mathcal{P}$-type dimers, while the concentrated solutions would be helpful for the formation of the $\mathcal{S}$-type dimers. Clearly, this kind of selection could not be attributed to energetics since both types of dimers are rather stable at the simulation temperature (0.140). The dynamics would be the possible reason. It is observed that the binding between two extended monomers are rather fast and cooperatively when being initiated, during the formation of $\mathcal{S}$-type dimers. The main difficulty is the encounter of the two extended chains. This searching could be eased in conditions of high concentration, which produces the increase of $P^{\mathcal{S}}$ toward high concentrations. The formation of $\mathcal{P}$-type dimers is different, which generally forms after the formation of one or two hairpins. Otherwise, two extended chains are more preferential to the $\mathcal{S}$-type conformations. Therefore, a sufficient time is required for one peptide to form a proper hairpin structure before the collision of two chains. This has been illustrated that $\tau_f^{\mathcal{P}}$ is statistically larger than $\tau_f^{\mathcal{S}}$ in Figure 9. This kind of requirement for a large free path can be more easily realized in dilute solutions. In fact, these two kinds of effects exist concurrently in solutions. The competition between them induces the different partitions under various concentrations. The phenomenon demonstrates that the concentration could also modulate the dynamic behaviors of the system.

The concentration selection for structures also happens for large-scale aggregations.[19,20] A globule aggregation would like to appear in low concentrations, but the fibrils would form in high concentrations. From the view of dimers, the fluctuation and irregularity in the $\mathcal{P}$-type dimeric structures in low concentrations would prevent the formation of order fibrils, and induces a non-specific globular aggregations. Differently, the sheet structures are more easier to align with some branches induced by the crosslink between chains. As a result, the selection by concentration on the dimeric forms would be helpful to induce a difference in form of aggregations, and produce various kinds of concentration-dependent forms of aggregates. Our simulations on the dimers provide us some insights on understanding the structural dependence of aggregations on the concentrations.

CONCLUSION

Based on our simulation on the single ionic self-complementary polyalanine-based peptide chain system, there is a competition during the folding process resulted from three factors in our model: hydrogen bonding, electrostatic interaction and the chain entropy. The competition among these effects can make dramatic differences in determining the most stable chain conformations. By increasing the relative strength of electrostatic interactions, we observed the peptide undergone a preference conversion from forming α-helix to β-hairpin conformation. With the knowledge that a lot of prion proteins experience the change of structure from α-helix-type to β-sheet-type, the transition for EAK16-IV peptide may give us some insights on those processes. Clearly, a preferential interaction would regularly desired for such a structural conversion, which might be implemented by the disulfide bonds or metal ions. Our example shows the basic physical requirement for such a structural conversion.

Another interesting issue discovered in our work is the concentration dependence of the dimerization processes. This is a kinetics-controlled process. As suggested in the *in vivo* folding studies, the concentration would be very large for proteins. Our studies suggest the importance of the crowded environments for the ordered dimerization when there are some the preferential interactions. This mechanism can also be applied in further experiments for the shape control of the self-organizing materials.

All in all, based on a model peptide system, we explore mechanism and controlling factors for the formation of the local structure and aggregations. The results suggest that the electrostatic interaction and crowded environment would be important for the formation of fibril aggregations of the peptides.

ACKNOWLEDGMENT

We thank Dr. Ding for helpful discussions on the method and models. The computational tasks are supported by Shanghai Supercomputer Center.

REFERENCES

1. Ellis RJ. Macromolecular crowding: an important but neglected aspect of the intracellular environment. Curr Opin Struct Biol 2001; 11:114–119.
2. Elli RJ. Macromolecular crowding: obvious but underappreciated. Trends Biochem Sci 2001;26:597–604.
3. Ellis RJ, Minton AP. Protein aggregation in crowded environments. Biol Chem 2006;387:485–497.
4. Nelson R, Eisenberg D. Structural models of amyloid-like fibrils. Adv Protein Chem 2006;73:235–282.
5. Dobson CM. Protein misfolding, evolution and disease. Trends Biochem Sci 1999;24:329–332.
6. Dobson CM. The structural basis of protein folding and its links with human disease. Phil Trans R Soc Lond B 2001;356:133–145.
7. Dobson CM. Protein folding and misfolding. Nature 2003;426:884–890.
8. Koo EH, Lansbury Jr. PT, Kelly JW. Amyloid diseases: abnormal protein aggregation in neurodegeneration. Proc Natl Acad Sci USA 1999;96:9989–9990.
9. Hardy J, Selkoe DJ. The amyloid hypothesis of Alzheimer's disease: progress and problems on the road to therapeutics Science 2002; 297:353–356.
10. Kreplak L, Aebi U. From the polymorphism of amyloid fibrils to their assembly mechanism and cytotoxicity. Adv Protein Chem 2006; 73:217–233.
11. Bemporad F, Calloni G, Campioni S, Plakoutsi G, Taddei N, Chiti F. Sequence and structural determinants of amyloid fibril formation. Acc Chem Res 2006;39:620–627.

12. Chiti F, Dobson CM. Protein misfolding, functional amyloid, and human disease. Annu Rev Biochem 2006;75:333–366.
13. Chi EY, Krishnan S, Randolph TW, Carpenter JF. Physical stability of proteins in aqueous solution: mechanism and driving forces in nonnative protein aggregation Pharm Res 2003;20:1325–1336.
14. Caplan MR, Moore PN, Zhang S, Kamm RD, Lauffenburger DA. Self-assembly of a β-sheet protein governed by relief of electrostatic repulsion relative van der waals attraction. Biomacromol 2000;1:627–631.
15. Lopez De La Paz M, Foldie K, Dobson CM. De novo designed peptide-based amyloid fibrils. Proc Natl Acad Sci USA 2002;99:16052–16057.
16. Zhang S, Rich A. Direct conversion of an oligopeptide from a β-sheet to an α-helix: a model for amyloid fomation. Proc Natl Acad Sci USA 1997;94:23–28.
17. Altman M, Lee P, Rich A, Zhang S. Conformational behavior of ionic self-complementary peptides. Protein Sci 2000;9:1095–1105.
18. Hong Y, Legge RL, Zhang S, Chen P. Effect of amino acid sequence and pH on nanofiber formation of self-assembling peptides EAK16-II and EAK16-IV. Biomacromol 2003;4:1433–1442.
19. Fung SY, Keyes C, Duhamel J, Chen P. Concentration effect on the aggregation of a self-assembling oligopeptide. Biophys J 2003;85: 537–548.
20. Jun S, Hong Y, Imamura H, Ha BY, Bechhoefer J, Chen P. Self-assembly of the ionic peptide EAK16: the effect of charge distributions on self-assembly. Biophys J 2004;87:1249–1259.
21. Nguyen HD, Hall CK. Spontaneous fibril formation by polyalanines: discontinuous molecular dynamics simulations. J Am Chem Soc 2006;128:1890–1901.
22. Hadama D, Yanagihara I, Tsumoto K, Engineering amyloidogenicity towards the development of nanofibrillar materials. Trends BioTech 2004;22:93–97.
23. Leffers K, Schell J, Jansen K, Lucassen R, Kaimann T, Nagel-Steger L, Tatzelt J, Riesner D. The structural transition of the prion protein into its pathogenic conformation is induced by unmasking hydrophobic sites. J Mol Biol 2004;344:839–853.
24. Takada S, Luthey-Schulten Z, Wolynes PG. Folding dynamics with nonadditive forces: a simulation study of a designed helical protein and a random heteropolymer. J Chem Phys 1999;110:11616–11629.
25. Smith AV, Hall CK. α-helix formation: discontinuous molecular dynamics on an intermediate-resolution protein model. Proteins: Struct Funct Genet 2001;44:344–360.
26. Ding F, Borreguero JM, Buldyrey SV, Stanley HE, Dokholyan NV. Mechanism for the α-helix to β-hairpin transition. Proteins: Struct Funct Genet 2003;53:220–228.
27. Ding F, Buldyrev SV, Dokholyan NV. Folding trp-cage to NMR resolution native structure using a coarse-grained protein model. Biophys J 2005;88:147–155.
28. Allen MP, Tildesley DJ. Computer simulation of liquids. New York: Oxford University, Press; 1989.
29. Chan HS, Dill KA. Protein folding in the landscape perspective: chevron plots and non-arrhenius kinetics. Proteins: Struct Funct Genet 1998;30:2–33.
30. Alder BJ, Wainwright TE. Studies in molecular dynamics, i: general method. J Chem Phys 1959;31:459–466.
31. Rapaport DC. Molecular dynamics simulation of polymer chains in solution. J Chem Phys 1979;71:3299–3303.
32. Zhou YQ, Karplus M. Folding thermodynamics of a model three-helix-bundle protein. Proc Natl Acad Sci USA 1997;94:14429–14432.
33. Smith SW, Hall CK, Freeman BD. Molecular dynamics for polymeric fluids using discontinuous potentials. J Comp Phys 1997;134: 16–30.
34. Andersen HC. Molecular dynamics simulatons at constant temperature and/or pressure. J Chem Phys 1980;72:2384–2393.
35. Zhou YQ, Karplus M. Equilibrium thermodynamics of homopolymers and clusters: molecular dynamics and monte carlo simulations of systems with square-well interactions. J Chem Phys 1997;107: 10691–10708.
36. Ferrenberg AM, Swendsen RH. Optimized monte carlo data analysis. Phys Rev Lett 1989;63:1195–1198.
37. Yang S, Cho SS, Levy Y, Cheung MS, Levine H, Wolynes PG. Domain swapping is a consequence of minimal frustration. Proc Natl Acad Sci USA 2004;101:13786–13791.
38. Ding F, Prutzman KC, Campbell SL, Dokholyan NV. Topological determinants of protein domain swapping. Struct 2006;14:5–14.
39. Chan HS. Modeling protein density of states: additive hydrophobic effects are insufficient for calorimetric two-state cooperativity. Proteins: Struct Funct Genet 2000;40:543–571.
40. Pain RH. Mechanisms of protein folding, New York; Oxford University Press; 2000.
41. Okamoto Y, Hansmann UHE. Thermodynamics of helix transitions studied by multicanonical algorithms. J Phys Chem 1995;99:11276–11287.
42. Lee IH, Kim SY and Lee J. Dynamic folding pathway models of α-helix and β-hairpin structures. Chem Phys Lett 2005;412:307–312.
43. Chakrabartty A, Baldwin RL. Stability of α-helices. Adv Protein Chem 1995;46:141–176.
44. Garcia AE, Sanbonmatsu KY. α-helix stabilzation by side chain shielding of backbone hydrogen bonds. Proc Natl Acad Sci 2002;99: 2782–2787.
45. Ma BY, Nussinov R. Stabilities and conformations of Alzheimer's β-amyloid peptide oligomers ($A\beta_{16-22}$, $A\beta_{16-35}$, and $A\beta_{10-35}$): sequence effects. Proc Natl Acad Sci USA 2002;99:14126–14131.